JOURNAL OF GEOPHYSICAL RESEARCH, VOL. 106, NO. B1, PAGES 721–739, JANUARY 10, 2001

Density structure of the lithosphere in the southwestern United States and its tectonic significance

Mikhail K. Kaban[1] and Walter D. Mooney

U.S. Geological Survey, Menlo Park, California

Abstract. We calculate a density model of the lithosphere of the southwestern United States through an integrated analysis of gravity, seismic refraction, drill hole, and geological data. Deviations from the average upper mantle density are as much as ±3%. A comparison with tomographic images of seismic velocities indicates that a substantial part (>50%) of these density variations is due to changes in composition rather than temperature. Pronounced mass deficits are found in the upper mantle under the Basin and Range Province and the northern part of the California Coast Ranges and adjacent ocean. The density structure of the northern and central/southern Sierra Nevada is remarkably different. The central/southern part is anomalous and is characterized by a relatively light crust underlain by a higher-density upper mantle that may be associated with a cold, stalled subducted plate. High densities are also determined within the uppermost mantle beneath the central Transverse Ranges and adjoining continental slope. The average density of the crystalline crust under the Great Valley and western Sierra Nevada is estimated to be up to 200 kg m^{-3} higher than the regional average, consistent with tectonic models for the obduction of oceanic crust and uppermost mantle in this region.

1. Introduction

The goal of this study is to use gravity data to construct a three-dimensional (3-D) density model of the lithosphere of the southwestern United States and to relate this model to tectonic processes. The study area includes all of California and Nevada; parts of Utah, Arizona, and Mexico, and the adjacent oceanic regions (Figure 1). We are able to remove the gravity effect of sedimentary basins and variations in crustal thickness owing to the availability of complementary information from seismic reflection profiles, well logs within sedimentary basins, and extensive seismic refraction measurements of crustal structure. The resulting residual anomalies reflect density inhomogeneities within the crystalline crust and uppermost mantle. These residual anomalies are further analyzed using an admittance method to estimate the depth of the inhomogeneities. From this analysis we obtain contour maps of density for both the crystalline crust and uppermost mantle relative to a reference model. These maps and cross sections illustrate the main features of the density structure of the lithosphere and correlate well with surface geology and tectonic history.

2. Initial Data

2.1. Gravity Data

The initial gravity data set has a grid spacing of 4 km containing Bouguer gravity values with terrain correction onshore [*Godson*, 1985] and free air anomaly (FAA) values offshore [*Simpson et al.*, 1986, Figure 1]. Bathymetric and topography data are also provided by *Simpson et al.* [1986]. We applied a Bouguer correction to the oceanic regions by calculating the gravitational effect of bathymetry and removing it from the free air anomaly. The resultant Bouguer gravity values interpolated on a $5' \times 5'$ grid are used in the following calculations.

2.2. Thickness and Density of Sediments

The first step in processing the Bouguer gravity map was to remove the large effect of extensive sedimentary basins, such as the Great Valley, which is ~700 km long and ~70 km wide. The thickness of low-density sediments used in these calculations is shown in Figure 2. A $2.5' \times 2.5'$ digital grid was prepared based on the data sources in Table 1. Basin thickness as great as 10 km is observed (Figure 2). Shallower basins are located offshore central and northern California. Although basins in western Washington and Oregon lie beyond the study area, they were also taken into account to avoid edge effects in the gravity calculations. We use the results by *Jachens and Moring* [1990] for the numerous but small-scale basins located in the Basin and Range Province.

To calculate the gravitational effect of sedimentary basins, it is necessary to estimate their density-depth structure. Numerous well logs in the study area provide data to 2–3 km depth. These data show complex variations in density with depth, including strong density contrasts [e.g., *Beyer et al.*, 1985]. However, owing to strong lateral variations, these density contrasts do not constitute regional structures. Therefore a reasonable approach is to construct a smooth density-depth relationship based on averaged borehole data and on well-determined density-compaction relations. This approach has been successfully used in previous gravity modeling of sedimentary basins [e.g., *Jachens and Moring*, 1990; *Langenheim and Jachens*, 1996; *Artemjev and Kaban*, 1994; *Artemjev et al.*, 1994].

The well logs show that bulk density is most affected by porosity and that the density of individual sedimentary grains is very close to the average upper crustal density of 2600–2700 kg m^{-3} [*Kennet et al.*, 1994; *Beyer et al.*, 1985; *McCulloh*, 1967]. According to well logs, the average density of sedimentary rocks exposed at the surface is ~1900–2000 kg m^{-3} on land

[1]Permanently at Institute of Physics of the Earth, Moscow.

Paper number 2000JB900235.

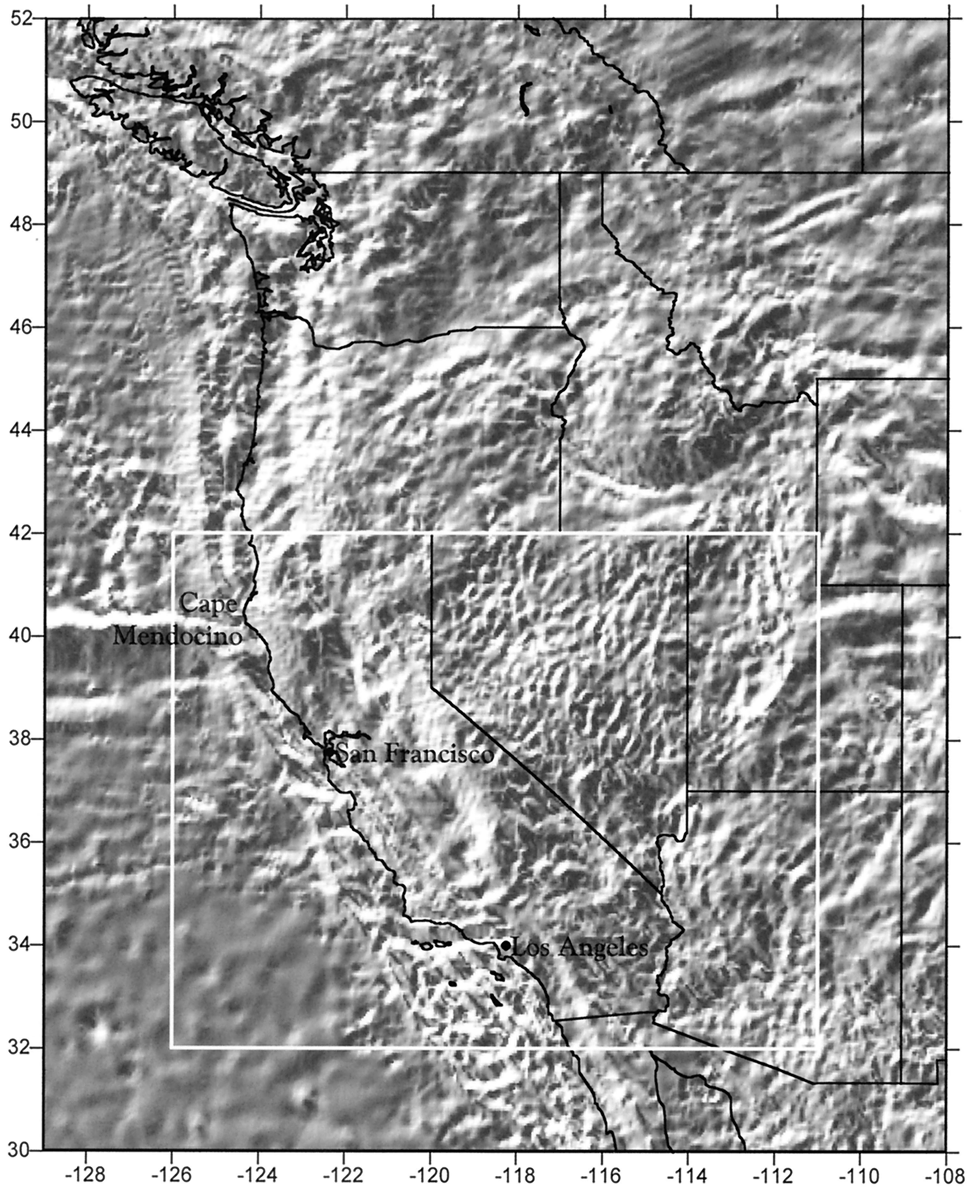

Figure 1. Regional gravity of the eastern Pacific and western North America. Free air anomaly is shown over the oceanic region, and Bouguer anomaly is shown over continents. The study area is indicated by the white rectangle (111°–126°W by 32°–42°N).

and slightly less beneath the Pacific Ocean. The density rapidly increases to 2100–2150 kg m^{-3} at ~500 m depth and continues to increase to ~2500 kg m^{-3} at 2.5–3.0 km depth [*Beyer et al.*, 1985; *Kennet et al.*, 1994]. Densities at greater depth are uncertain owing to sparse deep well log control. We adopt a smooth, nearly linear transition between a density of 2500 kg m^{-3} and the typical density (2650 kg m^{-3}) of high-grade metamorphic rocks at appropriate pressure (Figure 3). These results are consistent with models obtained from seismic refraction data that show a smooth velocity change in the lower sedimentary layer [*Holbrook and Mooney*, 1987]. Our empirical polynomial relationship (Figure 3) is used to estimate the gravitational effect of sediments in most of the study area. The exception is the narrow zone between the central California Coast Ranges and the Great Valley (Figure 2). This zone is filled by Cretaceous rocks with surface densities up to 2580 kg m^{-3} [*Irwin*, 1961]. Here we use a separate relation according to which the density is equal to 2550 kg m^{-3} at the surface and increases slightly with depth at a constant gradient of 10 kg m^{-3} km^{-1}.

Table 1. Main Data Sources for Sediment Thickness Map in Figure 2

Region	Reference
Base map for the whole area	*Frezon et al.* [1983]
Great Valley	*Jachens et al.* [1995]
Offshore basins	*Gardner et al.* [1992, 1993a, 1993b]
Basin and Range	*Jachens and Moring* [1990]
Los Angeles basin	*Fuis et al.* [1996] and *Langenheim and Jachens* [1996]

2.3. Variations in Crustal Thickness

The crustal thickness of the study area has been estimated from a compilation of seismic refraction results published through the year 1997 (Figure 4). The data sources are listed in Table 2. We assume a crustal thickness of 7.3 km for the crystalline oceanic crust beyond the continental shelf. There is an estimated 10% uncertainty in the calculated crustal thickness beneath seismic refraction profiles [*Mooney*, 1989]. For accurate calculations of the gravitational contribution of deep structures, such as variations in Moho depth, it is necessary to consider distances out to at least 10° (~1000 km) beyond the study area [*Artemjev et al.*, 1994]. Therefore we also digitized the crustal thickness map of North America [*Mooney and Braile*, 1989; *Mooney et al.*, 1998] and used this information in our calculations.

3. Crustal Gravity Anomalies and Residual Anomalies

3.1. Direct Gravity Calculations and the Crustal Gravity Field

After constructing maps for the two main crustal boundaries (basement and Moho depth) and assigning density values, we calculate the gravity effect of this simple model. We then remove this calculated field from the observed Bouguer gravity field to produce residual anomalies. We interpret the residual gravity field relative to a reference, one-dimensional density model. Our reference model is based on the summary of seismic refraction results by *Mooney and Weaver* [1989] (Table 3). The depth to Moho in the reference model corresponds to the average Moho depth (25 km) beneath the entire study area. An important parameter is the estimated density contrast at the Moho discontinuity. This density contrast may vary locally. However, gravity modeling shows that it is more appropriate to use first an average density contrast at the Moho and then to estimate lateral variations within a region [e.g., *Artemjev et al.*, 1994]. We have adopted an average crust-mantle density contrast of 420 kg m^{-3} (Table 3).

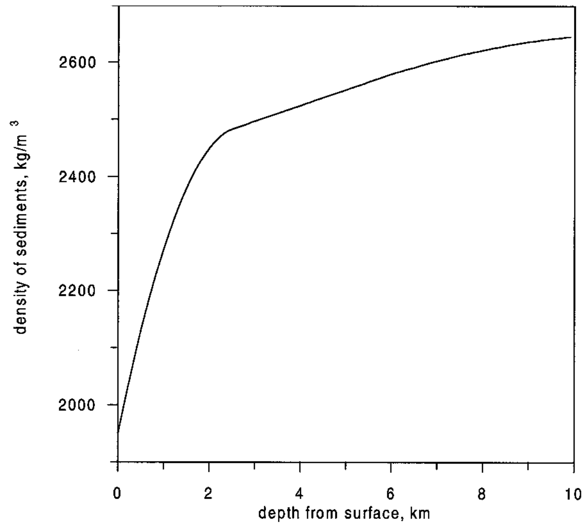

Figure 3. Density-depth relation for sediments based on well log and porosity data [*Kennet et al.*, 1994; *Beyer et al.*, 1985; *McCulloh*, 1967]).

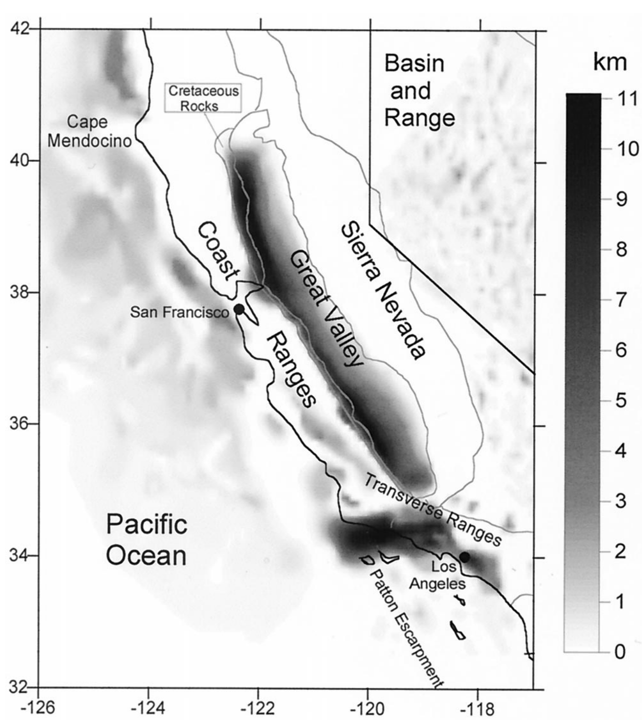

Figure 2. Thickness of low-density sediments and index map of the main physiographic provinces referred to in the text. Main data sources are listed in Table 1. The narrow zone on the western flank of the Great Valley is filled by Cretaceous rocks. The light lines show boundaries between the principal physiographic provinces of the study area.

The gravity anomaly of any layer within the Earth's crust and mantle is calculated using 3-D algorithms for a spherical Earth, taking into account changes of density in the horizontal and vertical direction and the average elevation of each cell. We compute the sum of the gravity influence of elementary volumes corresponding to the initial grids. We use the same algorithm as *Artemjev and Kaban* [1994] based on the formulas of *Strakhov et al.* [1989]. The estimated accuracy of the calculations is 1 mGal. The initial model is defined within the area enclosed by 30°–44°N and 108°–129°W. The calculated gravity field covers the smaller area enclosed by 32°–42°N and 111°–126°W. All model parameters and topography were prepared on the same $5' \times 5'$ grids. Within a radius of 222 km we use for the calculations the initial $5' \times 5'$ grids and outside this radius $1° \times 1°$ averaged data. The total radius of the direct gravity modeling is equal to 10° (1112 km) from each calculated point.

The resulting "sedimentary" gravity field varies from −75 to 0 mGal. The minimum value corresponds to the deepest parts of the Great Valley and basins in and around Los Angeles. The most important source of error for the calculated field is likely to be the assumed density-depth relation. We estimate this error to be ~15–20%. The "Moho gravity field" varies from −225 mGal for the Sierra Nevada to 260 mGal over the ocean. The sum of these two gravitational effects (sedimentary basins and Moho depth) represents a "predicted" Bouguer gravity anomaly field (Figure 5). Its long-wavelength component is mainly due to the Moho depth variations, while the sedimentary basins provide relatively short-wavelength anomalies.

3.2. Residual Anomalies

The residual anomaly field (Plate 1) is the observed Bouguer gravity field minus the two corrections discussed above. Resid-

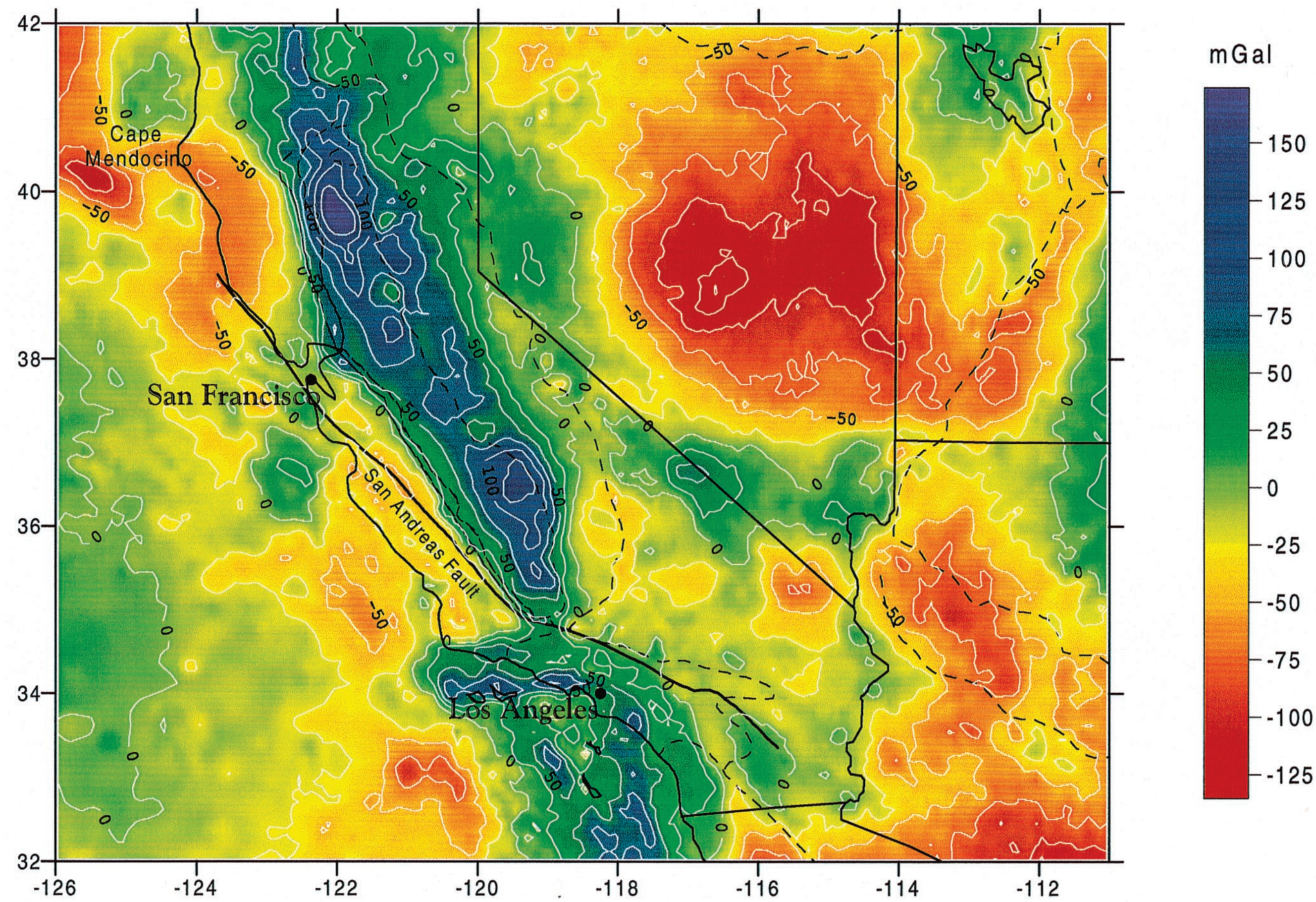

Plate 1. Residual gravity anomalies (mGal) obtained by removing the influence of sediments and variations in Moho depth (Figure 5) from the Bouguer gravity. Dashed lines show boundaries between principal physiographic provinces (see Figure 2), San Andreas fault (SAF) is indicated by a solid line.

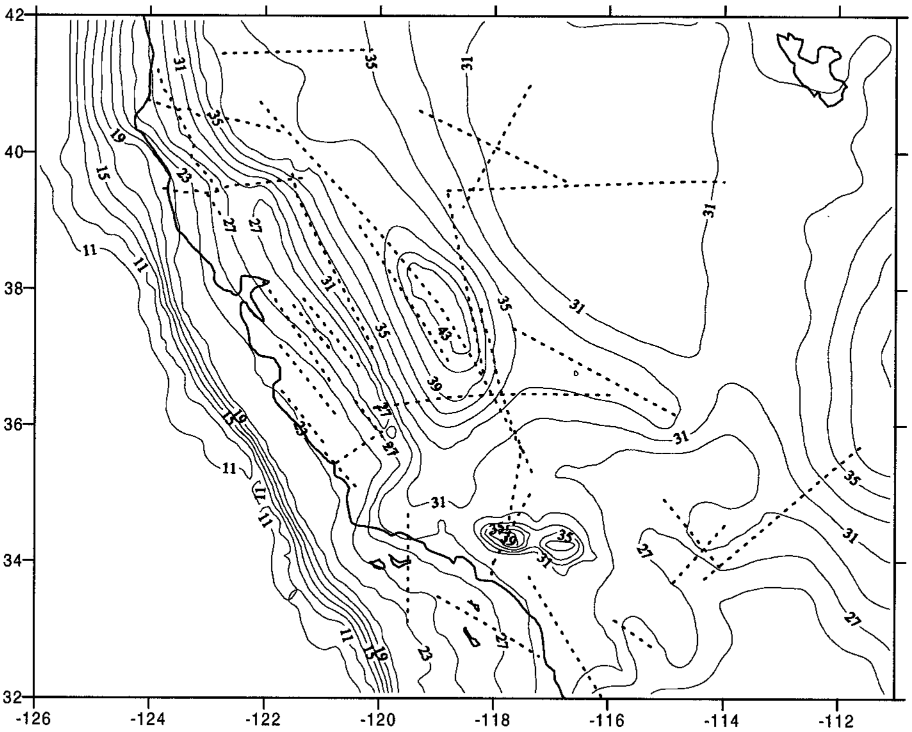

Figure 4. Moho depth (below sea level), 2-km contour intervals. Dashed lines indicate seismic profiles that provide control. Data sources are listed in Table 2.

ual anomalies are due to density inhomogeneities within the crust and uppermost mantle. The variation is large and ranges from approximately −150 to +150 mGal. The maximum error is conservatively estimated to be 25–30 mGal. The following features have amplitudes that significantly greater than the possible error: (1) a broad minimum of about −100 mGal located over the Basin and Range, (2) a strong maximum with an amplitude of up to +140 mGal over the Great Valley and the Sierra Nevada–Foothills Metamorphic Belt, (3) a gravity maximum (+80 mGal) in southern California beneath Los Angeles and an extensive offshore region, and (4) a gravity minimum (−60 mGal) in the northwestern part of the study area centered at 39.5°N by 123.5°W, south of Cape Mendocino.

The main sources of these anomalies may be located either in the crystalline crust or in the uppermost mantle. In section 4, an admittance analysis is performed to estimate the depth to anomalies.

Table 2. Main Data Sources for Moho Depth Map in Figure 4

Region	Reference
Base map for the study area	*Mooney and Weaver* [1989]
Sierra Nevada	*Fliedner et al.* [1996]
North American plate near Mendocino triple junction	*Beaudoin et al.* [1996]
Los Angeles basin, San Gabriel Mountains and adjoining area	*Fuis et al.* [1996]
Eastern Transverse Ranges	*Richards-Dinger and Shearer* [1997] and *Lamanuzzi* [1981]
Eastern and southern parts of the study area	*Mooney and Braile* [1989]

4. Isostatic Model of the Lithosphere of the Southwest United States

4.1. Residual Topography

High-amplitude residual anomalies indicate that isostatic compensation for near-surface density anomalies is not provided by crustal thickness variations, as would be predicted by simple Airy or elastic plate models. To investigate this, we consider the residual topography, a quantity that characterizes the isostatic state of the lithosphere. It is equivalent to the total sum of anomalous masses of the crustal column (with a total crustal load, p):

$$p = 2670t + (\rho_{\text{sed}} - 2700)s + 420(M_0 - M), \quad \text{km} \times (\text{kg m}^{-3}) \tag{1}$$

where

t topography (km);
s thickness of sedimentary basin (km);
ρ_{sed} average density of sediments (kg m^{-3});
M depth to Moho;
$M_0 = 25$ km.

All density values have units kg m^{-3}, and a value of 2670 kg m^{-3} is used for the topography above the sea level, 2700 kg m^{-3} for standard upper crust, and 420 kg m^{-3} for the density contrast across the Moho.

For oceanic crust, the density in (1) of 2670 kg m^{-3} must be replaced by 2700 − 1030 = 1670 kg m^{-3}. The parameter p is equivalent to the thickness (in km) of a layer with a density of (±)1000 kg m^{-3} that produces the same pressure as the lateral variations of the crustal model (Figure 6). Thus a regional component of the residual topography, p, represents the mass

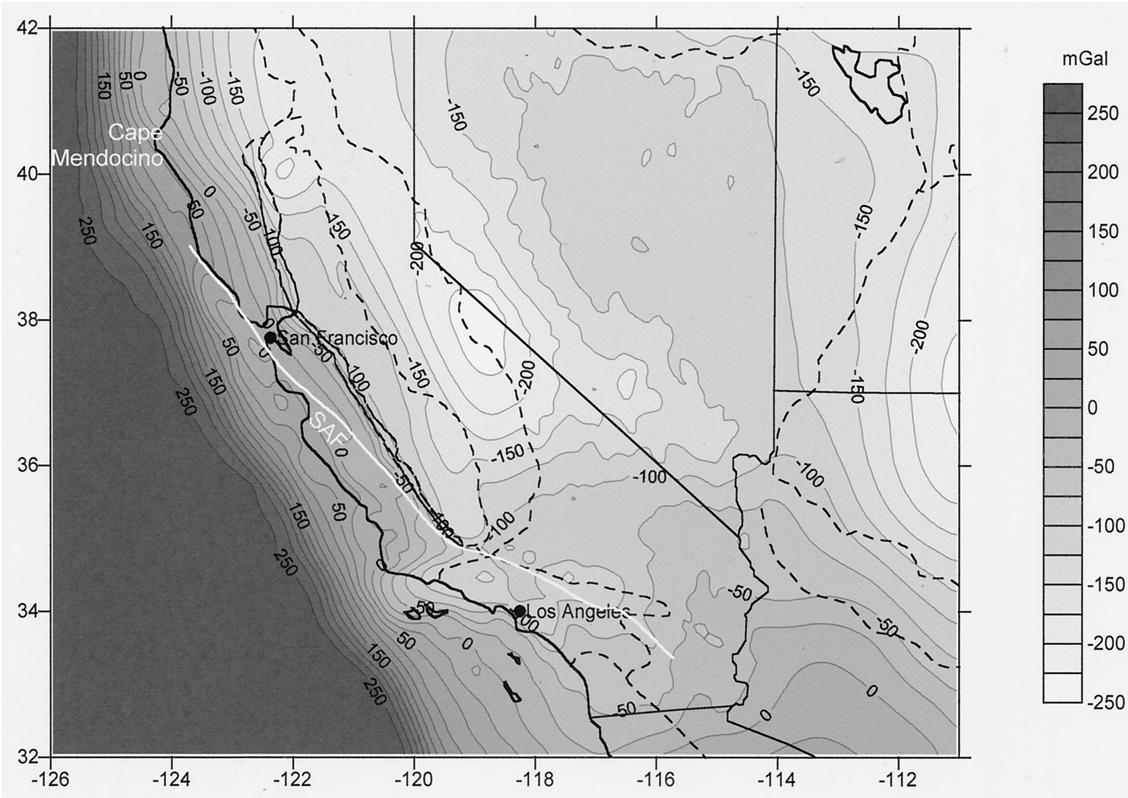

Figure 5. Total gravitational effect (mGal) due to low-density sediments and variations in Moho depth relative to the reference model. This gravity field is removed from the regional gravity field (Figure 1) to produce a residual gravity map (Plate 1). Dashed lines show boundaries between principal physiographic provinces (see Figure 2), San Andreas fault (SAF) is marked by solid white line.

that needs to be added (or subtracted) to the crust and upper mantle to provide isostatic equilibrium. Local features of p (for wavelengths <100–150 km) are likely to be elastically supported by the lithosphere.

4.2. Transfer Function (Admittance) Analysis of the Residual Anomalies and Residual Topography

Residual gravity and residual topography are here analyzed using the admittance (transfer function) technique. The procedure is similar to the way that Bouguer anomalies and surface topography are commonly analyzed to determine the style of isostatic compensation and depth of compensating masses. The residual topography may be considered as providing an anomalous pressure on the lithosphere. If the residual topography is in isostatic compensation, we may assume that the residual anomalies (reflecting the influence of the compensating masses) may be represented by the convolution of the residual topography (lithospheric load) p and a function f, the transfer function or admittance. Our approach is similar to that of *Dorman and Lewis* [1970], *McNutt* [1979], and *Sheffels and McNutt* [1986], who relate Bouguer or free air anomalies (FAA) to observed topography. We use the corresponding relation for residual anomalies and the residual topography:

$$\Delta g_{\mathrm{res}} = f^{*}p + \varepsilon, \quad (2)$$

where Δg_{res} is residual gravity, p is the residual topography estimated according to (equation (1)), asterisk signifies convolution, and ε is a "noise" component not correlated with the load. In the Fourier domain,

$$G_{\mathrm{res}} = FP + E. \quad (3)$$

The transfer function F reflects the style of isostatic compensation. Consequently, it is possible to draw conclusions regarding the isostatic compensation mechanism from admittance analysis. Appendix A describes a method to estimate the admittance within a localized area of arbitrary shape.

Admittance is often determined analytically using assumed compensation models. However, in some cases, there are inconsistencies between the theoretic admittance curves and direct calculations of density inhomogeneities [*Artemjev and Kaban*, 1987, 1991]. These differences can be caused, for example, by edge effects, the influence of the 3-D structures, or the nonlinearity of the isostatic density model. To evaluate our use

Table 3. Reference Density Model for Gravity Calculations

Layer	Depth, km	V_p,[a] km s^{-1}	Density,[b] kg m^{-3}
Upper crust	0–11.5	5.7–6.2	2700
Lower crust	11.5–25	6.6–7.2	2930
Upper mantle	>25	7.8–8.2	3350

[a] *Mooney and Weaver* [1989].
[b] Converted from velocity using relations from *Christensen and Mooney* [1995].

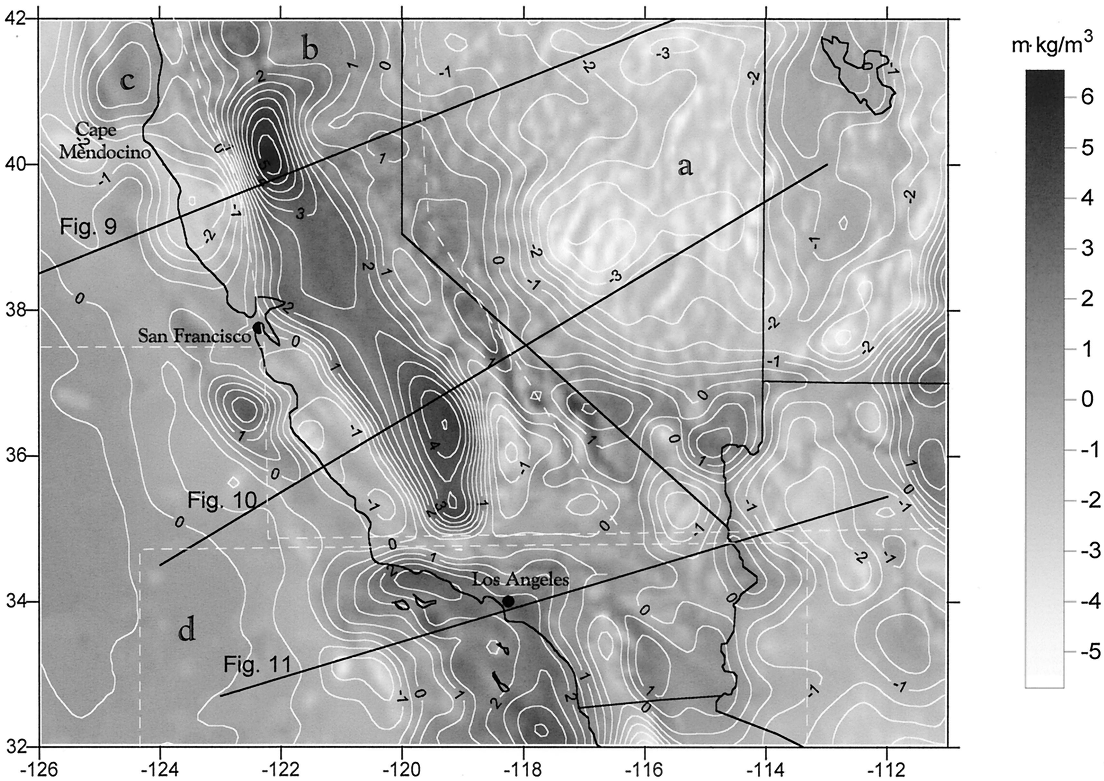

Figure 6. Additional compensating loads existing within the crust and uppermost mantle obtained after accounting for topography (water), sediments, and variations in Moho depth. These loads provide isostatic compensation for large-scale crustal structures, such as the broad, elevated Basin and Range Province. The plotted values (m (kg m^{-3})) are equivalent to the thickness (in km) of a layer with a density of ($\pm$) 1000 kg m^{-3}. This parameter is equivalent to the isostatic residual topography but with the opposite sign. The isolines are smoothed (the wavelengths <100 km are suppressed) to remove local features that are likely to be elastically supported by the lithosphere. The initial field is shown as a black and white image. White dashed lines indicate the main tectonic features for which admittance analysis was performed, letters a–d correspond to the graphs in Figure 8. Solid black lines indicate the positions of the cross sections shown in Figures 9–11.

of admittance analysis, we performed a test of the method, as described below.

We consider two alternative models for the distribution of the compensating masses within the crust and within the uppermost mantle. The crustal model places all compensating masses within the crystalline crust. The gravity field of this model is estimated by solving the direct gravity problem as described previously. The alternate mantle model places all compensating masses below the crust, to a depth known as the maximum depth of isostatic compensation, here assumed to be 90 km. We then compute the admittance for both models using residual gravity and residual topography. The four areas for which we performed the analysis are outlined by white dashed lines in Figure 6.

The admittance was calculated for the crustal isostatic model for four areas (Figure 7a), together with the theoretical admittance estimated assuming that the depth to the center of compensating masses is equal to 20 km. There exists a general correspondence of all curves for the wavelengths >90 km (Figure 7a) though some systematic differences are visible. Figure 7b demonstrates the admittance estimated for the mantle isostatic model. In this case the differences between the analytical and model curves are more significant, especially for the Basin and Range and for the area covering Great Valley and Sierra Nevada. Using the analytical curve for the isostatic model construction may lead to 15 km error in the determination of an average position of compensating masses.

To avoid possible influence of the effects described above, the transfer functions for different compensating models are determined by directly calculating the gravitational field for the density inhomogeneities in the model. We then apply the same algorithm as used for the observational admittance calculation but now using the model field instead of the residual anomalies. Therefore we may assume that possible distortions of the experimental and model admittance are the same and may directly compare them.

It is usually assumed that the shape of the transfer function is determined by the depth of the compensating masses and the effective elastic plate thickness. In our case, both the residual gravity and residual topography are computed taking into account the real positions of the main density boundaries, which in turn reflect elastic deformation. Nonzero flexural rigidity may cause either an increase or a decrease in the experimental transfer function values. Some examples of the transfer function for the residual gravity and topography in the case of nonzero flexural rigidity are shown in Figure 7c. Theoretical details for their computation are provided in Appendix A. An additional (hidden) load p_{hid}, which is not included in the initial density model, is located at the depth of 40 km in all cases. The solid line shows the reference curve for a zero value

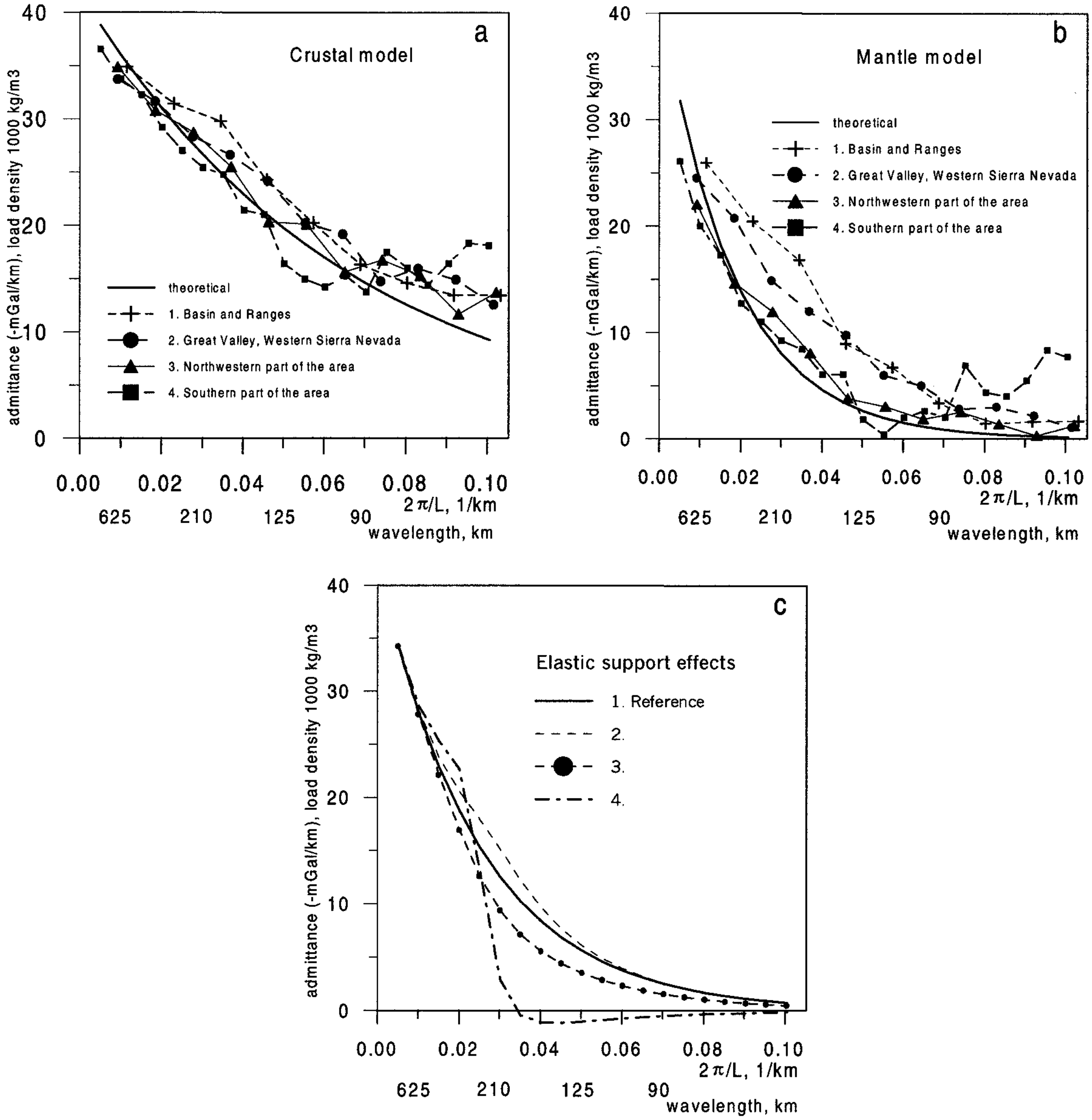

Figure 7. (a) Admittance curves for the isostatic model in which compensating masses are placed within crystalline crust ("crustal model," see text for more details). Solid line is computed analytically assuming that the average depth to the compensating masses is equal to 20 km. Lines 1–4 are computed based on the model gravity field for selected areas using the same technique as for the experimental admittance calculation. (b) Admittance curves for the mantle isostatic model according to which compensating masses are within in the upper mantle. (c) Examples of a model transfer function for the residual gravity and topography in the case of nonzero flexural rigidity computed from equation (A7) in Appendix A. Hidden load is located at 40 km in all cases. The noise level is constant $\beta_{noise} = 1$. Line 1 (solid) is a reference curve for a zero value of the elastic plate thickness. Line 2 corresponds to the case where there is no correlation between the external and hidden loads ($\beta_{obs} = 0$). Line 3 represents the case when the hidden load is negatively correlated with the observed one ($\beta_{obs} = -2$). Line 4 shows the admittance when the hidden load is positively correlated with the observed one ($\beta_{obs} = 2$).

of the elastic plate thickness. Line 2 corresponds to the case when there is no correlation between the external load p_{ext} (topography and the low density of sediments) and the hidden load p_{hid}. These values slightly exceed the reference ones at the midrange wavelengths. The third admittance in Figure 7c was computed for the case when the hidden load is negatively correlated with the observed one. This case may correspond to the Great Valley or the Basin and Range Province. The fourth curve in Figure 7c corresponds to the case of positive correlation between the observed and hidden loads. This admittance is unstable and exceeds the reference curve at the longest wavelengths but abruptly drops to zero at midwavelength.

In the present study we are mostly concerned with the determination of the depth of the density anomalies in the crust and uppermost mantle. It is well known that elastic response of the lithosphere leads to an abrupt decrease in coherence between the residual anomalies and residual topography at short wavelengths. Therefore we restrict the admittance analysis to

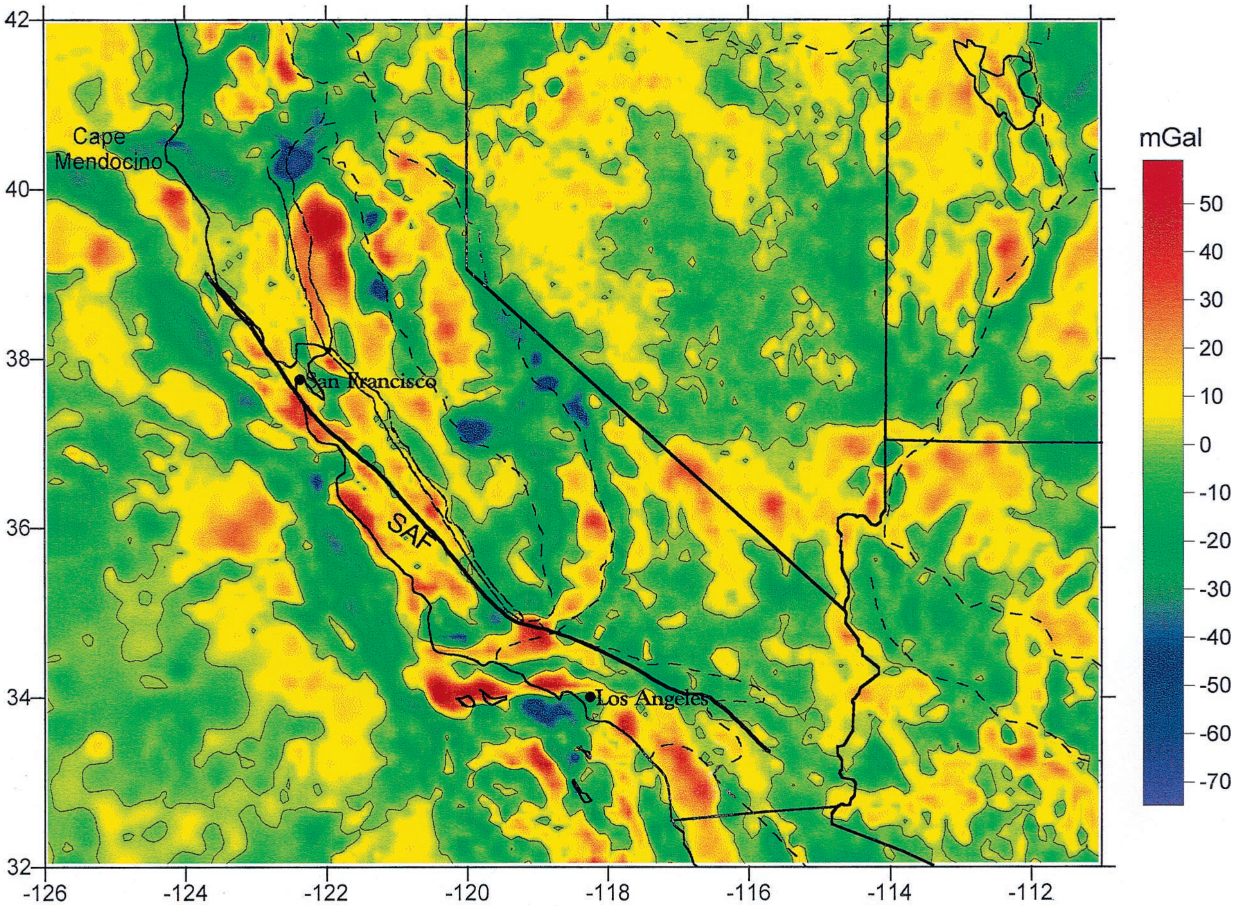

Plate 2. Isostatic gravity anomalies obtained by removing from the residual anomalies (Plate 1) the gravity field of the best fitting isostatic model. This map may be compared with the isostatic gravity map of *Simpson et al*. [1986] (see text for discussion). Dashed lines show boundaries between principal physiographic provinces (see Figure 2), San Andreas fault (SAF) is indicated by a solid line.

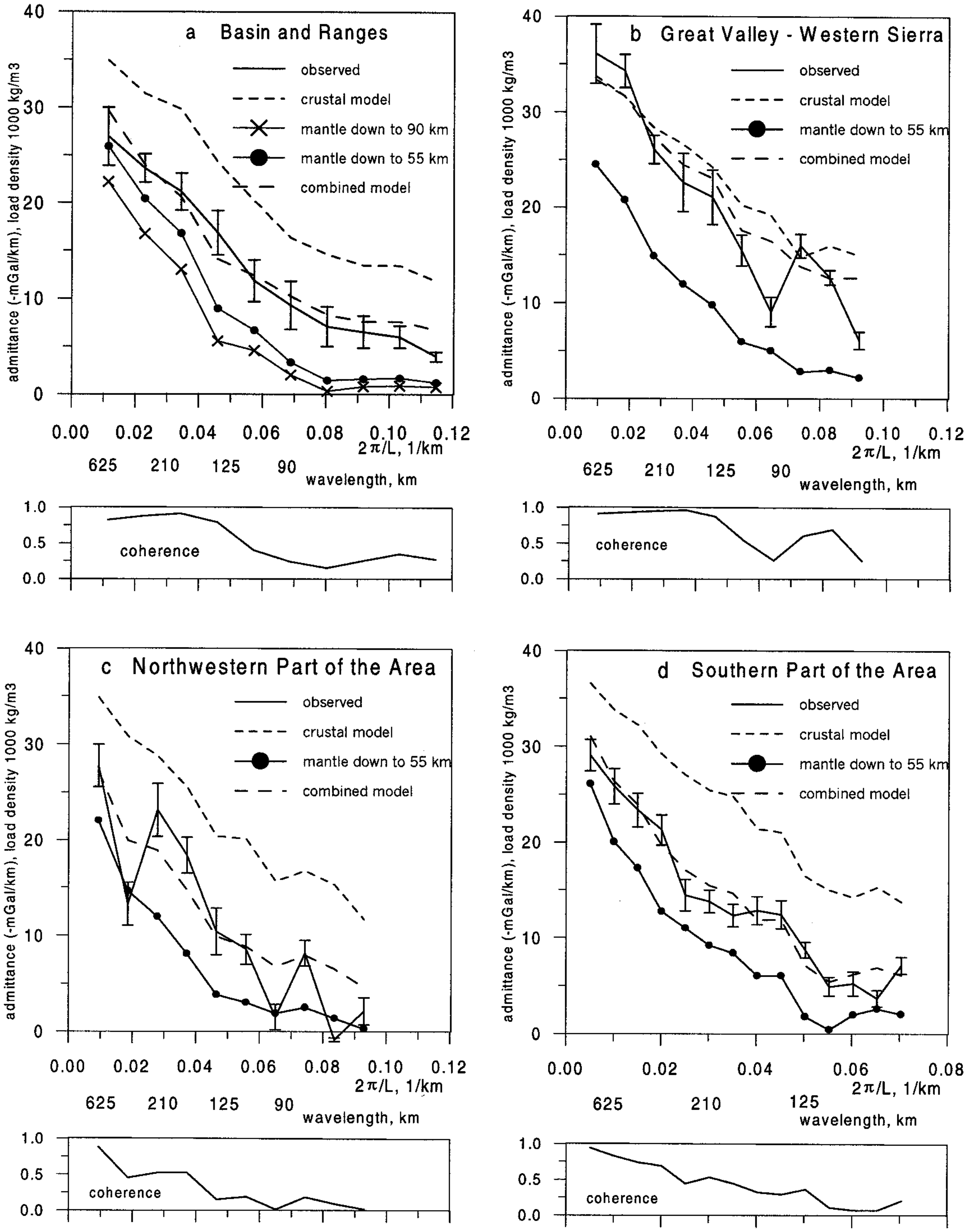

Figure 8. Observed and calculated admittance of the residual anomalies and residual topography obtained for the principle physiographic provinces shown in Figure 6: (a) Basin and Range Province, (b) the Great Valley, Western Sierra Nevada, and Foothills Metamorphic Belt, (c) northwestern part of the study area, including the northern California Coast Ranges, and (d) southern part of the study area, including the Los Angeles basin and Transverse Ranges.

large wavelengths (>100–170 km, depending on the area) where the coherence exceeds 0.4. The results obtained for the areas containing the most pronounced and reliable residual anomalies (Plate 1 and Figure 6) are discussed below.

4.2.1. Basin and Range Province. The Basin and Range Province is characterized by a pronounced low in the residual gravity field (Plate 1 and Figure 6). Figure 8a shows the observed and several predicted values for admittance curves corresponding to different assumed models for the distribution of compensating masses. The curve for pure crustal compensation lies systematically above the observed values. This indicates that the actual compensating masses are primarily located below the crust. The curve for mantle compensation to a depth of 90 km is well below the observed curve, and the curve for a mantle compensation depth of 55 km is closer to, but still well below, the observations. Thus the best fitting model appears to be intermediate between the crustal and mantle models. One model that satisfies the observed data has ~80% of compensating masses within the mantle to a depth of 55 km, with the remainder in the crust ("combined model," Figure 8a). It is possible to vary the depths to the compensating crustal and subcrustal masses, but the principal characteristic of the model requires that most of the low-density anomaly be located in the uppermost mantle. Elastic deformation of the lithosphere due to the subcrustal load is not visible in the experimental admittance values. This agrees with the results of *Bechtel et al*. [1990], who obtained an extremely low value of the effective elastic plate thickness (4 km) for the Basin and Range Province.

4.2.2. Great Valley–western Sierra Nevada and Foothills Metamorphic Belt. The Great Valley and western flank of the Sierra Nevada in California have a pronounced residual gravity high. It is difficult to find a simple isostatic compensation model for this region whose admittance is close to the observed values throughout the whole range of wavelengths (Figure 8b). This may be due to the fact that the structures are characterized by a substantial departure from local isostasy, as indicated by the abrupt decrease in the observed admittance values with decreasing wavelength (Figure 8b). Nevertheless, for wavelengths >150 km the admittance is fit better by either the crustal or the combined compensation models (Figure 8b). The combined model for this area has 80% of the compensation within the crust, indicating a primarily crustal origin for the residual gravity anomaly. The crustal origin of this anomaly is also consistent with the high horizontal gravity gradients exhibited in this area (Plate 1).

4.2.3. Northwestern California. A local residual gravity minimum exists in northwestern California at 39.5°N by 123.5°W, 100 km south of Cape Mendocino. The theoretical admittance values for purely crustal compensation are significantly higher than the observed values (Figure 8c). Our best fitting model is similar to the compensation model for the Basin and Range Province (80% mantle, 20% crust; Figure 8c). In this region, relatively high horizontal gradients (Plate 1) are consistent with compensation in the mantle because the crust-mantle boundary is rather shallow. Thus it appears that most of this residual gravity minimum is caused by low densities within the uppermost mantle. A tectonic interpretation is that this low density corresponds to a "slabless window" filled with relatively hot asthenospheric mantle material, as discussed below.

4.2.4. Southern California continental shelf (Borderlands). Los Angeles and the offshore region (the California Borderlands) are characterized by a clear residual gravity high (Plate 1 and Figure 6). Theoretical admittance values (Figure 8d) show that a crustal compensation model fails to explain the observed admittance values. The best fitting model is one in which the main part (~70%) of the compensation is within the uppermost mantle, though crustal features may locally be important. The Moho boundary is not everywhere well determined by seismic data; thus a significant part of this positive anomaly may be explained by an upward shift of the estimated depth to Moho.

4.3. New Isostatic Anomaly Map

Isostatic anomalies have been previously calculated for the whole territory of the United States [*Simpson et al*., 1986], and short-wavelength anomalies have been successfully used for the interpretation of crustal structure [e.g., *Jachens and Moring*, 1990; *Griscom and Jachens*, 1990]. The isostatic map of *Simpson et al*. [1986] uses a simple isostatic compensation model. This model assumes Airy compensation of topography, with a constant density 2670 kg m^{-3}. In calculating a new isostatic anomaly map we include (1) the previously described data for the sedimentary basins, (2) determinations of the depth of the Moho boundary from seismic refraction studies, and (3) crustal and upper mantle density anomalies determined from admittance analysis.

The total field of the best fitting model of crustal and mantle density described in section 4.2 was subtracted from the residual anomaly map, resulting in an isostatic residual gravity anomaly map. In addition we removed the long-wavelength influence of topography beyond 167 km (the radius of the Bouguer correction) [*Kaban et al*., 1999]. The final isostatic anomaly map is shown in Plate 2. In this new map the regional maximum identified by *Simpson et al*. [1986] in the near offshore is eliminated because of more complete inclusion in the density structure of the ocean crust. Other differences exist over the Great Valley, Coast Ranges, and Sierra Nevada.

4.4. Density Model of the Crystalline Crust and Upper Mantle

The computed isostatic anomalies (Plate 2) still contain the effect of unknown density inhomogeneities in the crystalline crust and their compensation in the mantle. These are generally not correlated with the residual topography shown in Figure 6. We apply an inversion method based on Fourier transformations to determine these additional inhomogeneities. The algorithm used is similar to that proposed by *Cordell et al*. [1991] for the determination of "decompensating" gravity anomalies. We may reliably determine only the integrative effects of crustal inhomogeneities and their compensation, which is assumed to be in the upper mantle. Average depths to these sources are the main parameters that control the solution (see Appendix A). To provide stability to the inversion, we restrict it to wavelengths of 150–1000 km. The average depths to the anomalous masses within the crust and mantle are assumed to be 15 and 50 km, respectively.

We use uniform depths of 15 and 50 km for crustal and subcrustal loads, respectively. These values are reasonable for the continental area, while the oceanic crust is thinner than 15 km. Thus additional crustal densities determined by the inversion of the isostatic anomalies may be overestimated by up to 70% in ocean areas. Fortunately, the most significant variations of the isostatic anomalies occur onshore. Maximum perturbation to the initial isostatic density model does not exceed 50% offshore; thus maximum total error may be ~30%. The anomalous densities obtained after this inversion of the isostatic anomalies have been added to the initial isostatic lithosphere model.

Plate 3a shows the resulting anomalous density distribution in the crystalline crust. These density anomalies are spread over the entire crustal thickness, thus representing average crustal density inhomogeneities. A more geologically plausible body would be thinner and consequently have a higher density. The most pronounced feature in this map is an elongate maximum of up to 200 kg m^{-3} located in the Great Valley and western Sierra Nevada (Plate 3a). Subcrustal density inhomogeneities are shown in Plate 3b. Well-defined minima are located within the Basin and Range Province and in northwestern California, south of Cape Mendocino (at 39°N by 123.5°W;

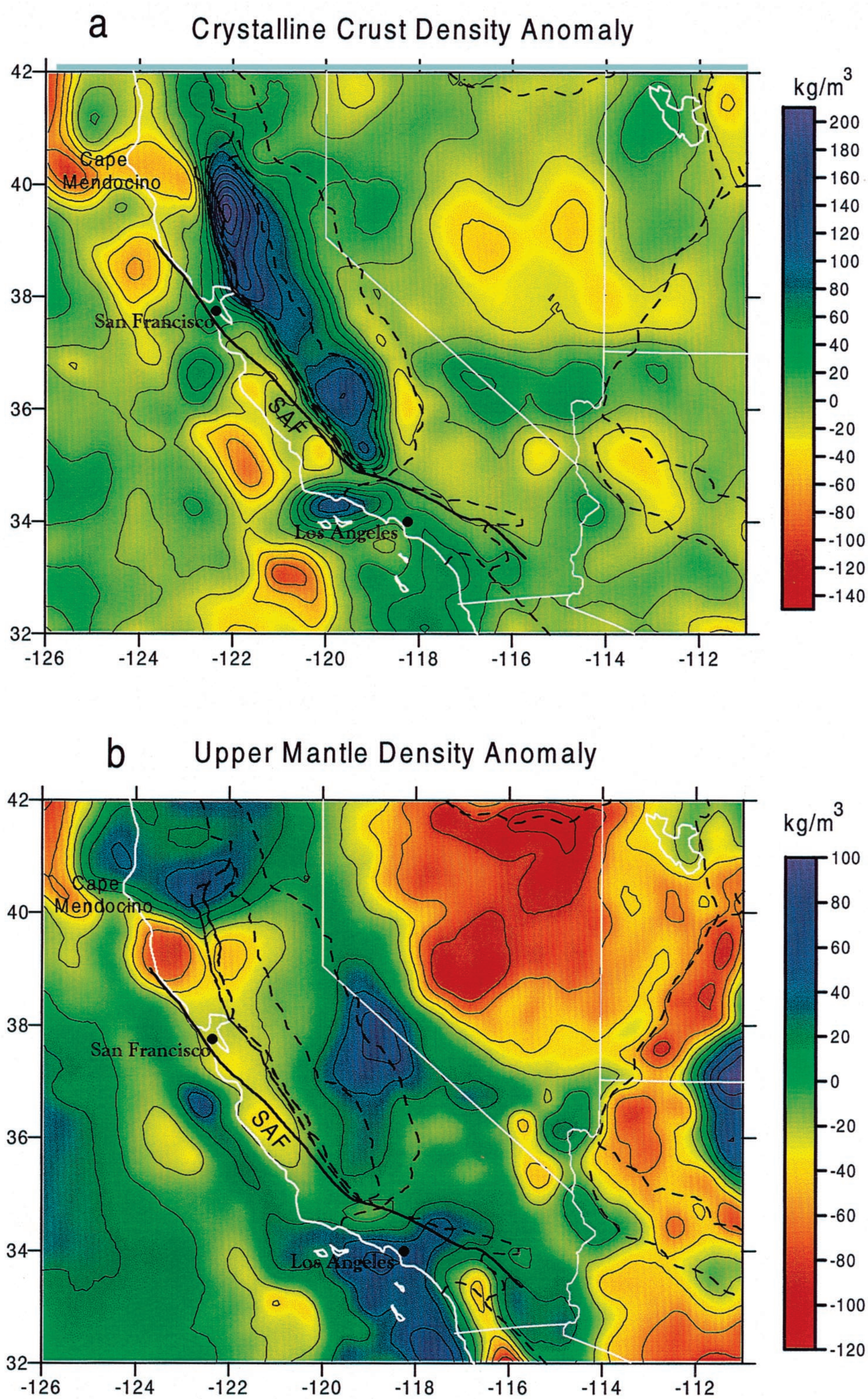

Plate 3. (a) Density anomalies within the crystalline crust from the isostatic lithosphere model and an inversion of isostatic anomalies. Dashed lines show boundaries between principal physiographic provinces (see names in Figure 2). San Andreas fault (SAF) is indicated by a solid line. (b) Density anomalies within the uppermost mantle from the isostatic lithosphere model and an inversion of isostatic anomalies. Dashed lines show boundaries between principal physiographic provinces (see Figure 2). San Andreas fault (SAF) is indicated by a solid line.

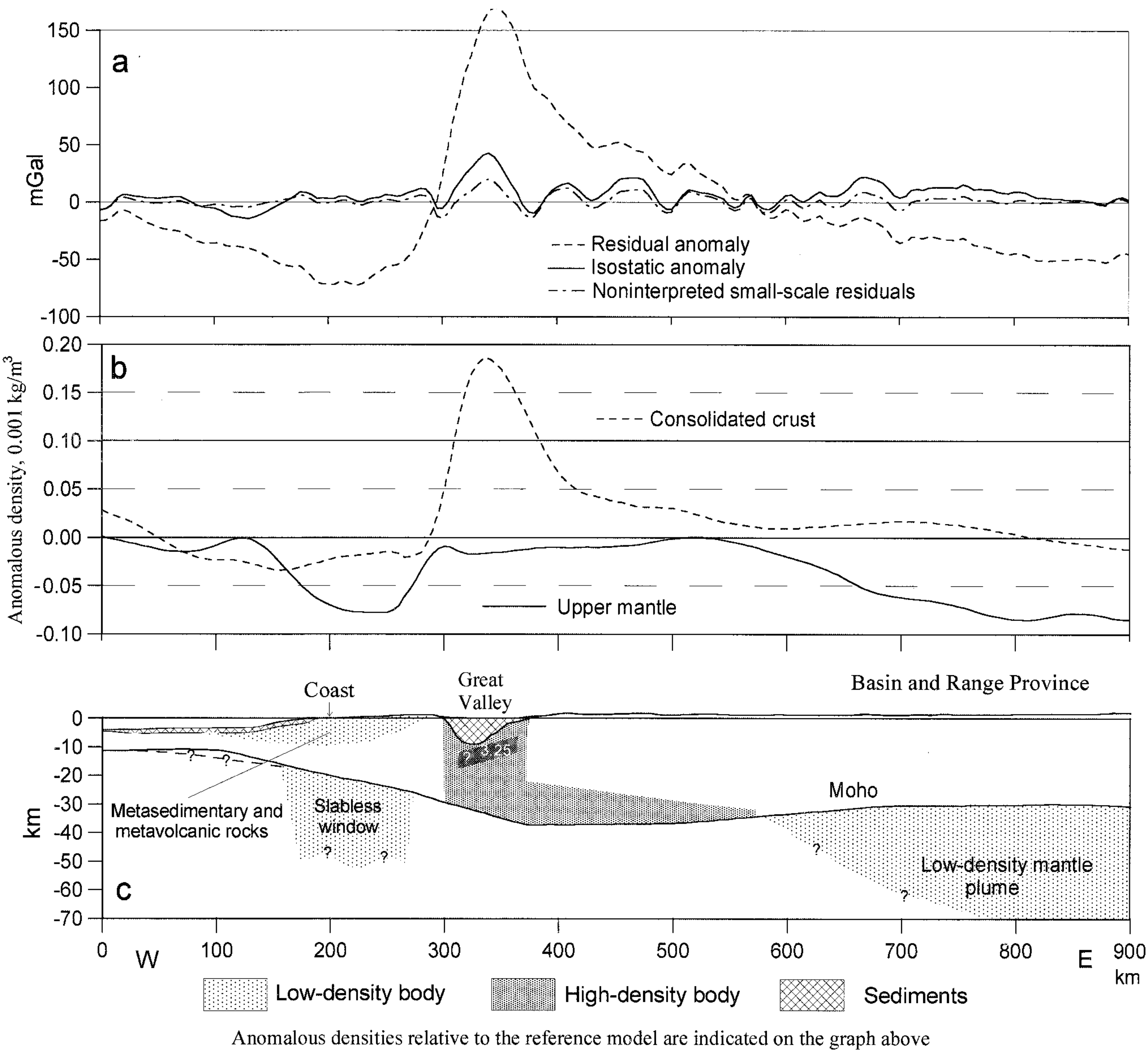

Figure 9. Lithosphere cross section across northern California from the Pacific Ocean to the Basin and Range Province. Location is shown in Figure 6. (a) Gravity anomalies used to determine density structure of the crust and upper mantle. The residual anomalies reflect the total effect of crustal and upper mantle density perturbations to the initial model. The isostatic anomalies represent disturbances to the calculated isostatic lithosphere model. (b) Average density perturbations to the initial model of the crust and upper mantle obtained by the inversion of the residual and isostatic anomalies. (c) Schematic lithospheric cross-section with inferred high- and low-density blocks.

Plate 3b). Significant positive anomalies in the uppermost mantle are located (1) in the middle of the study area, beneath the central part of the Great Valley and Sierra Nevada, (2) in southern California beneath the Los Angeles basin and adjacent offshore region, and (3) north of 40°N in California (Plate 3b). We will discuss each of these anomalies.

5. Tectonic Significance of Gravity Models

5.1. Density Structure of the Uppermost Mantle

Our results indicate that the density of the upper mantle is very heterogeneous. Density variations correspond to ±3% of the absolute density value (Plate 3b). The same relative percent variations were found for the compressional wave velocity, V_p, in the upper mantle of this region from seismic tomography studies [*Benz et al.*, 1992; *Humphreys and Dueker*, 1994a]. As discussed by *Humphreys and Dueker* [1994b], the $V_p - \rho$ temperature-dependent scaling factor is

$$(1/\rho_0)(\delta\rho/\delta T)/(1/V_0)(\delta V_p/\delta T),$$

and ranges from 0.1 to 0.4 for the T-P conditions in the uppermost mantle of the western United States. The lower value (0.1) is for the case of partial melting and corresponds to a more pronounced decrease in V_p as compared with ρ. For a temperature-scaling factor of 0.4, a significant part (60%) of the upper mantle density variations could be due to changes in

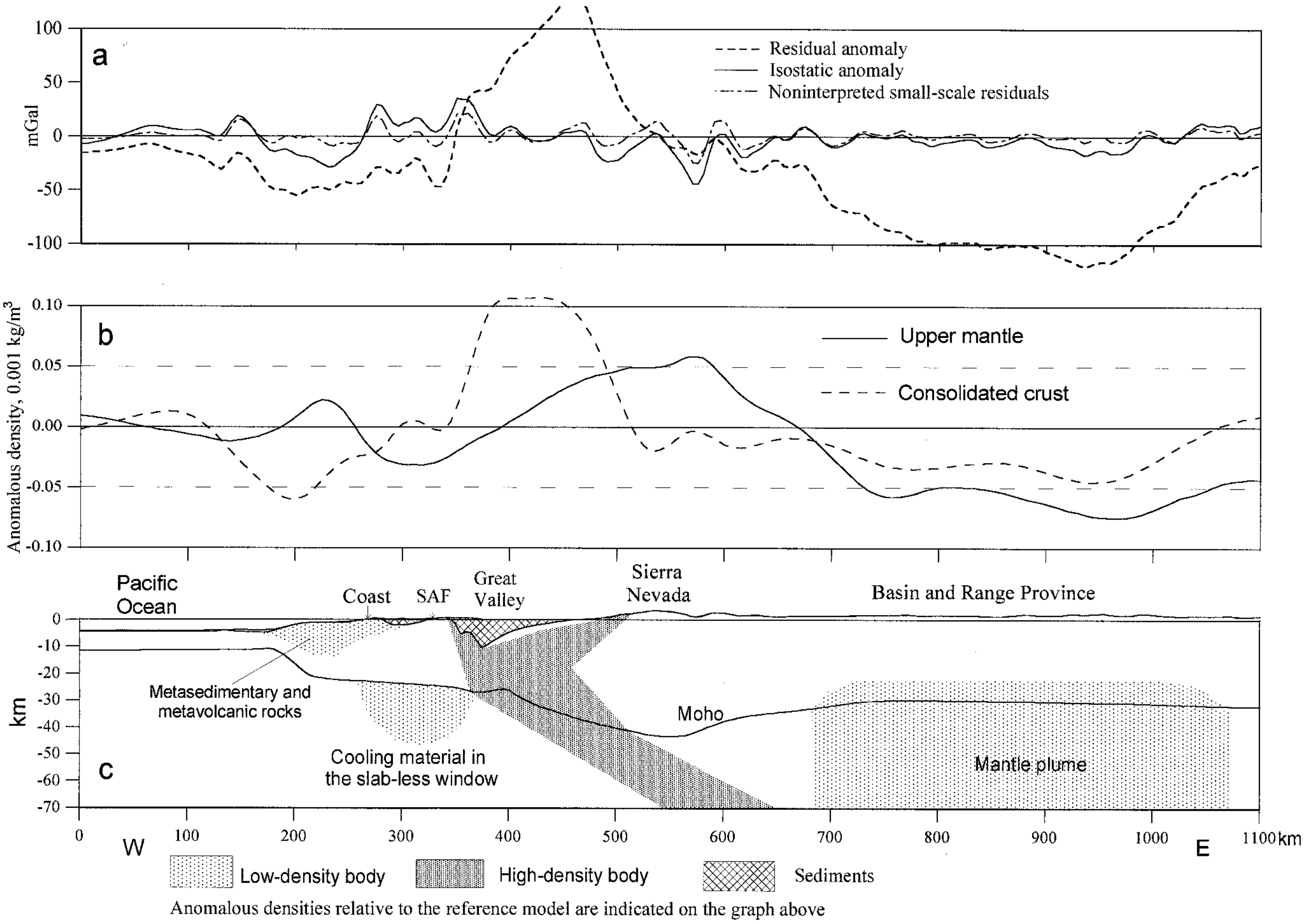

Figure 10. Lithosphere cross-section and data across central California from the Pacific Ocean to the Basin and Range Province. Location is shown in Figure 6. (a) Gravity anomalies used to determine density structure of the crust and upper mantle. (b) Average density perturbations to the initial model of the crust and upper mantle obtained by the inversion of the residual and isostatic anomalies. (c) Schematic lithospheric cross section with inferred high- and low-density blocks.

chemical (mineralogic) composition. *Humphreys and Dueker* [1994b] provide a thorough discussion of the likely origin of such compositional variations.

5.2. High Density Crystalline Crust Under the Great Valley and Western Sierra Nevada

The NW-SE oriented residual anomaly over the Great Valley–western Sierra Nevada is the most prominent positive anomaly (Plate 1). As was shown in section 4.2.2, its source is located within or above the lower crust (Plate 3a). This implies that the average density of the entire crystalline crust under the Great Valley must be at least 80–220 kg m^{-3} higher than in the reference model (Table 3). The corresponding absolute density is 3000–3150 kg m^{-3} (Figure 9). Thus parts of the crystalline crust here are composed of mafic and ultramafic rocks, a conclusion arrived at by previous workers [*Cady*, 1975; *Simpson et al.*, 1986; *Godfrey et al.*, 1997]. Seismic refraction data show crustal *P* wave velocities >7 km s^{-1} in the central part of the Great Valley [*Colburn and Mooney*, 1986; *Holbrook and Mooney*, 1987; *Godfrey et al.*, 1995, 1997]. Previous gravity and magnetic studies have also indicated that the western part of the Sierra Nevada and the eastern part of the Great Valley contain high-density crustal blocks [*Oliver*, 1980; *Jachens et al.*, 1995; *Godfrey et al.*, 1997]. Our results show that this must be true for a much larger area. The maximum of the residual anomalies (Plate 1) and corresponding high-density crustal block (Plate 3a) cover the entire area from the western part of the Sierra Nevada to the western edge of the Great Valley. This result differs from teleseismic images that place the main high-velocity body within the upper mantle beneath this region [*Benz et al.*, 1992; *Humphreys and Dueker*, 1994a]. The tomographic results may not have succeeded in imaging the high-velocity crust due to the compensating effect of the low-velocity sediments, combined with limited station spacing.

Two alternative hypotheses have been proposed to explain the crustal structure of the Great Valley and adjoining area. One hypothesis is that it is oceanic in nature (a fragment of Farallon plate [*Bailey et al.*, 1964; *Hamilton*, 1969; *Cady*, 1975; *Griscom et al.*, 1993]). Alternatively, it may consist of a westward extension of the Sierra Nevada batholith and the Sierra Nevada–Foothills metamorphic complex [*Mooney and Weaver*, 1989; *Ramirez*, 1993]. Our results favor the first hypothesis, and show that the crustal density under the Great Valley is too high to be associated with typical continental rocks of the Sierra Nevada–Foothills Metamorphic Belt. In fact, the gravity anomalies are so strongly positive as to require the existence of dense mantle material within the crust beneath the Great Valley, a conclusion previously arrived at by *Godfrey et al*. [1997, 1998] based on seismic refraction and gravity data. It is also significant that the western edge of the gravity maximum is sharp while the eastern one is smooth (Plate 1). This suggests that the high-density crustal block may be inclined beneath the Sierra Nevada (Figures 9 and 10). *Oliver et al*. [1993] found that average surface densities in the western Sierra Nevada vary from 2600 to 2850 kg m^{-3}. The higher values are significantly greater than normal upper crustal densities (2700 kg m^{-3}). Thus it is possible to explain 20–25% of the positive residual anomaly by high densities in the upper crust, with an additional thick sheet (slab) of high density in the lower crust, as indicated in Figures 9 and 10.

5.3. Basin and Range Province

Admittance analysis shows that the broad and deep minimum (−150 mGal) in the residual anomalies located over the Basin and Range Province is mainly produced by low-density mantle (Plate 3b). The corresponding density deficit is about −100 kg m^{-3}. The location of this minimum corresponds to regions of low upper mantle seismic velocity and high heat flow [e.g., *Thompson et al*., 1989]. However, the admittance result indicates that the main sources of buoyant upper mantle are concentrated within the uppermost mantle, 20–40 km below the Moho, while the seismic and thermal anomalies may extend much deeper. It is not possible to explain the velocity and density decrease solely by elevated temperatures or partial melting because the relative density decrease will be significantly less than the corresponding velocity decrease [*Humphreys and Dueker*, 1994b]. Thus we suggest that ~70–80% of the decrease in the upper mantle density is due to a change in composition, possibly due to the intrusion of relatively low-density basalt into the warm uppermost mantle.

5.4. Subducted Gorda Plate and Slabless Window

The "slab window" model, derived assuming rigid plate geometry, proposes that the North American plate slides off the top of the subducting Gorda/Juan de Fuca plate as this plate moves north with the Mendocino Triple Junction [e.g., *Atwater*, 1989]. The resulting gap (slab window) is filled by upwelling asthenospheric material [*Dickinson and Snyder*, 1979; *Jachens and Griscom*, 1983]. Our results are consistent with this model. The positive upper mantle density anomaly located in the northwestern part of the study area (north of 40°N; Plate 3b) marks the position of the subducted Gorda plate, while the prominent minimum located to the south (Plate 3 and Figure 9) indicates the position of the slabless window. This minimum is somewhat wider than is imaged in the seismic tomographic study of *Benz et al*. [1992]. The region of low mantle density covers the northern part of the Coast Ranges and a small offshore area. In the extreme northwestern part of the study area it appears to merge into the minimum under the Gorda Ridge (Plate 3b). The northern boundary of the slabless window is sharp, while the southern boundary is very smooth and appears to extend into the southern Coast Ranges. The magnitudes of the density and velocity perturbations correspond well with the above mentioned velocity-density temperature scaling factor, thereby providing support for a cooling model for the slabless window.

5.5. Density Structure of the Sierra Nevada

We have found significant variations in the density of the upper mantle beneath the Sierra Nevada (Plate 3). A broad region of remarkably dense upper mantle (+60 kg m^{-3}; Plate 3b) underlies the central portion of the range at 37.5°–38°N. The region of high density is oriented roughly N-S along 119°W, and the southern portion correlates very well with a high-velocity mantle anomaly reported by *Benz et al*. [1992], *Biasi and Humphreys* [1992], and *Benz and Zandt* [1993]. These high densities are not matched by high seismic velocities immediately below the Moho [*Fliedner et al*., 1996; *Ruppert et al*., 1998], which suggests that the density anomaly is located some distance (>10 km) below the Moho. The upper mantle density maximum may be explained by the presence of a cold, stalled plate, the extension of a plate fragment hypothesized to underlie the Great Valley (Figure 10).

5.6. Southern California: Transverse Ranges, Adjacent Offshore Region, and San Andreas Fault

High-density mantle is imaged beneath the central Transverse Ranges and adjacent continental shelf (Plate 3b). The eastern part of this density maximum correlates with a high-velocity body within the mantle detected by teleseismic methods beneath the Transverse Ranges [*Raikes*, 1980; *Humphreys and Clayton*, 1990; *Humphreys and Dueker*, 1994a]. This body has been interpreted as resulting from lithospheric subduction associated with crustal convergence [*Sheffels and McNutt*, 1986; *Humphreys and Hager*, 1990]. The high-density upper mantle beneath the continental shelf and Los Angeles region is of uncertain origin. It may have arisen from tectonic underplating (stacking) of a cold, shallow-dipping subducted oceanic lithosphere (Figure 11).

The San Andreas fault (SAF) marks a major plate boundary in the study area. The southern part of the SAF up to approximately 35.5°N latitude coincides approximately with the eastern boundary of the relatively high-density crust (Plates 1 and 3a). To the north, the SAF is west of the high-density crust of the Great Valley. These observations are consistent with those determined from teleseismic images [*Benz et al*., 1992]. Thus the location of the SAF appears to correlate with, and perhaps be controlled in part by, the subsurface geology, particularly the upper and middle crustal composition, as reflected in the residual gravity anomaly map (Plate 1) and map of average crustal density (Plate 3a). The density of the crystalline crust is a proxy for its bulk composition, with higher densities correlating with rheologically stronger, quartz-poor compositions. Higher-density crustal blocks will therefore behave more rigidly compared with low-density crustal blocks.

6. Conclusions

We have estimated the density structure of the crystalline crust and uppermost mantle of the southwestern United States from an analysis of gravity data. We find a clear correlation with regional geology and tectonics. We have used admittance analysis to separate mass anomalies in the crystalline crust and upper mantle. Density variations in the upper mantle are ±3% of the average reference value (3350 kg m^{-3}). A consideration of the temperature-dependent scaling of seismic velocity and density, together with the results from seismic tomography, indicates that these density variations cannot be explained solely by thermal effects. A substantial part (more than 50%) of these variations must be due to variations in chemical (mineralogic) composition. We hypothesize that these variations are related to the existence of (1) cold, stalled subducted

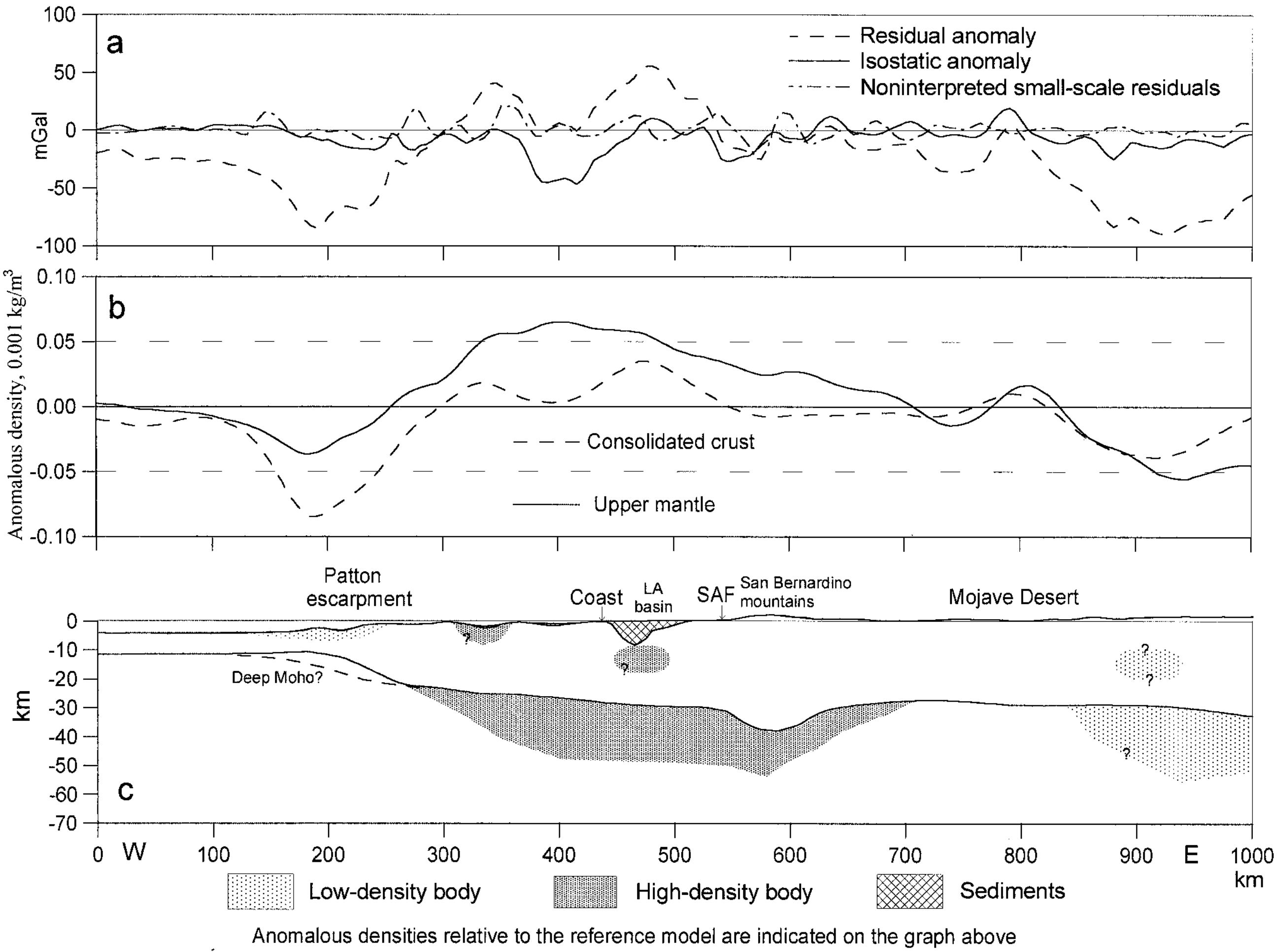

Figure 11. Lithospheric cross section and data across southern California from the Pacific Ocean to the Mojave Desert. Location is shown in Figure 6. (a) Gravity anomalies used to determine density structure of the crust and upper mantle. (b) Average density perturbations to the initial model of the crust and upper mantle obtained by the inversion of the residual and isostatic anomalies. (c) Schematic lithospheric cross section with inferred high- and low-density blocks.

plates, (2) obducted oceanic crust and uppermost mantle, and (3) shallow, upwelling asthenosphere.

The broad minimum in residual gravity anomalies (up to -150 mGal) located over the Basin and Range Province is due to low densities (-100 kg m^{-3}) within the uppermost mantle. The low-density region is concentrated 20–30 km below the Moho and may in part reflect relatively low-density basaltic sills intruded into uppermost mantle during late Cenozoic Basin and Range extension.

The density structure of the northern Sierra Nevada differs remarkably from the central and southern Sierra Nevada. A relatively low-density crust underlain by a dense upper mantle characterizes the anomalous central/southern part. The locally dense upper mantle may be due to a stalled subducted plate. The recent uplift of the Sierra Nevada indicates that the stalled plate is decoupled from the overlying crust.

High densities are found within the upper mantle beneath the greater Los Angeles region and adjoining continental slope. Similar to the central/southern Sierra Nevada, these high densities may be due to a cold lithospheric plate associated with an earlier episode of subduction.

The average density of the crystalline crust under the Great Valley and western Sierra must be up to 200 kg m^{-3} higher than the regional average. This result supports previous hypotheses based on seismic, gravity, and magnetic data that parts of this region are underlain by obducted oceanic crust and uppermost mantle [*Godfrey et al.*, 1997].

The subducted Gorda plate and the slabless window are imaged by a dipole anomaly in the northwestern part of the study area [*Jachens and Griscom*, 1983]. A positive anomaly marks the location of the subducting Gorda plate. A pronounced negative anomaly (-60 kg m^{-3}) is detected in the upper mantle under the northern part of the Coast Ranges and adjacent ocean (near the position 37.5°N by 123.5°W). This anomaly is probably due to the upwelling of asthenospheric material within the slabless window.

Appendix

A1. Experimental Admittance Determination

Experimental admittance values $F(k)$ are usually determined using Fourier transforms of the gravity anomalies $G(k)$

and the load (topography) $P(k)$. Following *Dorman and Lewis* [1970] and *Sheffels and McNutt* [1986]:

$$F(k) = \mathrm{Re}\,\langle G(\boldsymbol{k})P^*(\boldsymbol{k})\rangle/\langle P(\boldsymbol{k})P^*(\boldsymbol{k})\rangle, \qquad \text{(A1)}$$

$$k = \sqrt{k_x^2 + k_y^2}$$

where the angle brackets indicate averaging of the 2-D Fourier transforms over the discrete wavenumber bands to reduce the influence of noise. The asterisk indicates the complex conjugate. A specific transfer function (admittance) is obtained for each tectonic area. The expression (A1) may not always be applied directly, especially when the configuration of the region under study is nonrectangular, and thus it is difficult to use direct Fourier transformations. Instead, we compute the autocovariance (γ_{pp}) and cross-covariance (γ_{gp}) functions of the residual topography and residual gravity. The averaged spectra in (A1) can then be found by averaging the cross covariance and autocovariances over the discrete bands of the radius vector **r**, followed by a Hankel transformation [*Arfken*, 1968]:

$$\langle P(\boldsymbol{k})P^*(\boldsymbol{k})\rangle = \int_0^\infty \langle \gamma_{pp}(r_x, r_y)\rangle r J_0(kr)\, dr$$
$$\langle G(\boldsymbol{k})P^*(\boldsymbol{k})\rangle = \int_0^\infty \langle \gamma_{gp}(r_x, r_y)\rangle r J_0(kr)\, dr, \qquad \text{(A2)}$$

where $r = \sqrt{r_x^2 + r_y^2}$, and J_0 is the zero-order Bessel function.

Cross covariances and autocovariances may be determined for an area of any shape (theoretically even for disconnected areas). It is also significant that the cross covariances and autocovariances are center-weighted functions. It is easier to reduce edge effects during their transformation into cross and power spectra than while making Fourier transformations of the gravity and topographic data.

A2. Inversion of the Isostatic Anomalies

Residual isostatic anomalies contain the effect of still unknown crustal density inhomogeneities p_{crust} (the internal crustal load, equal to the anomalous density multiplied by the crystalline crustal thickness) and their compensation by mantle density anomalies whose total sum is equal to p_{crust} but with the opposite sign. Following *Cordell et al.* [1991] we assume that the total gravity effect (residual isostatic anomalies) in the Fourier domain is as follows:

$$F[\Delta g(x, y)] = 2\pi G F[p_{\mathrm{crust}}(x, y)] \cdot [\exp(-kZ_{\mathrm{crust}}) - \exp(-kZ_{\mathrm{root}})], \qquad \text{(A3)}$$

$$\delta\rho_{\mathrm{mantle}} = -p_{\mathrm{crust}}/H_{\mathrm{mantle}}$$

where

- Z_{crust} average depth to the crustal load location, equal to 15 km;
- Z_{root} average depth to the mantle compensating masses, equal to 50 km;
- G gravitational constant;
- p_{crust} $\delta\rho_{\mathrm{crust}} \cdot H_{\mathrm{crust}}$;
- k wavelength, equal to $2\pi/L$, L;
- H_{mantle} thickness of the upper mantle layer providing additional compensation;
- F Fourier transform, with other parameters as above.

Determination of the inner crustal load and corresponding density variations from equation (A3) is an unstable inverse gravity problem for short and long wavelengths [*Cordell et al.*, 1991]. To provide a stable solution, we restrict it to the wavelength interval of 150–1000 km.

A3. Transfer Function for the Residual Anomalies and Residual Topography (Elastic Plate Model)

Let us assume that p_{obs} is the observed load represented mainly by topography and anomalous density of sediments, p_{hid} is the hidden load which may be of a different origin, and D is flexural rigidity of the lithosphere. Then the amplitude of the deformation of the elastic plate under both the observed and hidden load and expressed in Fourier domain depending on the wavenumber k is [e.g., *McNutt*, 1979; *Sheffels and McNutt*, 1986]

$$M(k) = [P_{\mathrm{ext}}(k) + P_{\mathrm{hid}}(k)]/(k^4 D + \Delta\rho g), \qquad \text{(A4)}$$

where $\Delta\rho$ is density contrast at the base of the plate that is assumed to be at the Moho, and g is gravitational acceleration. The residual topography combines the effect of the observed load, the total deformation, and an error of determination of this deformation (Moho variations) which is the most significant source of noise:

$$P(\boldsymbol{k}) = \frac{P_{\mathrm{obs}}(\boldsymbol{k}) - \Delta\rho g[P_{\mathrm{obs}}(\boldsymbol{k}) + P_{\mathrm{hid}}(\boldsymbol{k})]}{(k^4 D + \Delta\rho g) + P_{\mathrm{noise}}(\boldsymbol{k})}. \qquad \text{(A5)}$$

The residual gravity field combines the effect of the hidden load and an artificial effect introduced by the noise component due to the errors in the determination of the lithosphere boundaries:

$$G_{\mathrm{res}}(\boldsymbol{k}) = 2\pi G[P_{\mathrm{hid}}(\boldsymbol{k}) + P_{\mathrm{noise}}(\boldsymbol{k})] \exp(-kZ), \qquad \text{(A6)}$$

where Z is depth to the hidden load which is taken for simplicity to be equal to the depth of the artificially introduced density inhomogeneities P_{noise}. The noise component is not correlated with the observed and hidden load, and the noncorrelated part of the observed load may be attributed to the noise component. The admittance for the residual anomalies and the residual topography may be obtained by substituting (A5) and (A6) into (A1) and averaging over the orientation of vector k. After some simplifications and excluding of the second-order terms we obtain the admittance for the residual anomalies and residual topography:

$$F(k) \approx 2\pi G \exp(-kZ)(Q_f(k) + \beta^2_{\mathrm{noise}})/(Q_f^2(k) + \beta^2_{\mathrm{noise}}), \qquad \text{(A7)}$$

$$\beta_{\mathrm{noise}}(k) = \sqrt{\langle |P^2_{\mathrm{noise}}(\mathbf{k})|\rangle/\langle |P^2_{\mathrm{hid}}(\mathbf{k})|\rangle},$$

$$Q_f(k) = \frac{1 - \beta_{\mathrm{obs}} k^4 D/(\Delta\rho g)}{1 + k^4 D/(\Delta\rho g)},$$

$$\beta_{\mathrm{obs}}(k) = P_{\mathrm{obs}}(k)/P_{\mathrm{hid}}(k),$$

where β_{noise} is noise level relative to the hidden load, β_{obs} is relation of the observed and hidden load ($\beta_{\mathrm{obs}} = 0$ when the observed and hidden loads are not correlated), and $Q_f(k)$ is term related to the elastic support ($Q_f = 1$ when $D = 0$).

Acknowledgments. We are grateful to R. C. Jachens for providing valuable advice regarding this work. R. W. Simpson, R. J. Blakely, T. G. Hildenbrand and G. S. Fuis provided constructive suggestions and assistance with compiling background information. B. Hager, A. Levander, G. Humphreys, K. Favret, G. S. Chulick, R. Girdler and R. Mereu suggested improvements to the text. The Earthquake Hazards Reduction Program of the U.S. Geological Survey supported the first author as a visiting scientist while preparing this report. Discussions with Jim Mori, Lucy Jones, and J. R. Filson are appreciated. S. Detweiler helped to prepare the final version of the paper.

References

Arfken, G., *Mathematical Methods for Physicists*, Academic, San Diego, Calif., 1968.

Artemjev, M. E., and M. K. Kaban, Isostasy and the cross-spectral method of its study, *Phys. Solid Earth*, Engl. Transl., *23*, 935–945, 1987.

Artemjev, M. E., and M. K. Kaban, Isostatic and intracontinental orogenesis, *J. Geodyn*., *13*, 77–86, 1991.

Artemjev, M. E., and M. K. Kaban, Density inhomogeneities, isostasy and flexural rigidity of the lithosphere in the Transcaspian region, *Tectonophysics*, *240*, 281–297, 1994.

Artemjev, M. E., M. K. Kaban, V. A. Kucherinenko, G. V. Demjanov, and V. A. Taranov, Subcrustal density inhomogeneities of the northern Eurasia as derived from the gravity data and isostatic models of the lithosphere, *Tectonophysics*, *240*, 248–280, 1994.

Atwater, T., Plate tectonic history of the northeast Pacific and western North America, in *The Geology of North America*, vol. N, *The Eastern Pacific Ocean and Hawaii*, edited by E. L. Winterer, D. M. Hussong, and R. W. Decker, pp. 21–73, Geol. Soc. of Am., Boulder, Colo., 1989.

Bailey, E. H., W. P. Irwin, and D. L. Jones, Franciscan and related rocks and their significance in the geology of western California, *Bull. Calif. Div. Mines Geol*., *183*, 177 pp., 1964.

Beaudoin, B. C., et al., The transition from slab to slabless: Results from the 1993 Mendocino Triple Junction seismic experiment, *Geology*, *24*, 367–370, 1996.

Bechtel, T. D., D. W. Forsyth, V. L. Sharpton, and R. A. F. Grieve, Variations in effective elastic thickness of the North American lithosphere, *Nature*, *343*, 636–638, 1990.

Benz, H. M., and G. Zandt, Teleseismic tomography: Lithospheric structure of the San Andreas fault system in northern and central California, in *Seismic Tomography: Theory and Practice*, edited by H. M. Iyer and K. Hirahara, pp. 440–465, Chapman and Hall, New York, 1993.

Benz, H. M., G. Zandt, and D. H. Oppenheimer, Lithospheric structure of northern California from teleseismic images of the upper mantle, *J. Geophys. Res*., *97*, 4791–4807, 1992.

Beyer, L. A., S. L. Robbins, and F. G. Clutson, Basic data and preliminary density and porosity profiles for twelve borehole gravity surveys made in the Los Angeles, San Joaquin, Santa Maria and Ventura Basins, California, *U.S. Geol. Surv. Open File Rep*., *85-42*, 67 pp., 1985.

Biasi, G. P., and E. D. Humphreys, *P*-wave image of the upper mantle structure of central California and southern Nevada, *Geophys. Res. Lett*., *19*, 1161–1164, 1992.

Cady, J. W., Magnetic and gravity anomalies in the Great Valley and western Sierra Nevada metamorphic belt, California, *Spec. Pap., Geol. Soc. Am*., *168*, 56 pp., 1975.

Christensen, N. I., and W. D. Mooney, Seismic velocity structure and composition of the continental crust: A global view, *J. Geophys. Res*., *100*, 9761–9788, 1995.

Colburn, R. H., and W. D. Mooney, Two-dimensional velocity structure along the synclinal axis of the Great Valley, California, *Bull. Seismol. Soc. Am*., *76*, 1305–1322, 1986.

Cordell, L., Y. A. Zorin, and G. R. Keller, The decompensative gravity anomaly and deep structure of the Rio Grande Rift, *J. Geophys. Res*., *96*, 6557–6568, 1991.

Dickinson, W. R., and W. S. Snyder, Geometry of subducted slabs related to San Andreas transform, *J. Geol*., *87*, 609–627, 1979.

Dorman, L. M., and B. T. R. Lewis, Experimental isostasy, 1, Theory of determination of the Earth's isostatic response to a concentrated load, *J. Geophys. Res*., *75*, 3357–3365, 1970.

Fliedner, M. M., S. Ruppert, and The Southern Sierra Nevada Continental Dynamics Working Group, Three-dimensional crustal structure of the southern Sierra Nevada from seismic fan profiles and gravity modeling, *Geology*, *24*, 367–370, 1996.

Frezon, S. I., T. M. Finn, and J. H. Lister, Total thickness of sedimentary rocks in the conterminous United States, *U.S. Geol. Surv. Open File Rep*., *83-920*, 1983.

Fuis, G. S., et al., Images of crust beneath southern California will aid study of earthquakes and their effects, *Eos Trans. AGU*, *77*, 173, 176, 1996.

Gardner, J. V., et al., Map showing sediment isopachs in the deep-sea basins of the Pacific continental margin, Point Conception to Point Loma, *U.S. Geol. Surv. Misc. Invest. Map*, *I-2089-A*, 1992.

Gardner, J. V., et al., Map showing sediment isopachs in the deep-sea basins of the Pacific continental margin, Cape Mendocino to Point Conception, *U.S. Geol. Surv. Misc. Invest. Map*, *I-2090-A*, 1993a.

Gardner, J. V., et al., Map showing sediment isopachs in the deep-sea basins of the Pacific continental margin, Strait of Juan de Fuca to Cape Mendocino, *U.S. Geol. Surv. Misc. Invest. Map*, *I-2091-A*, 1993b.

Godfrey, N. J., B. C. Beaudoin, C. Lendl, A. Meltzer, and J. Luetgert, Mendocino triple junction seismic experiment, northern California, *U.S. Geol. Surv. Open File Rep*., *95-275*, 87 pp., 1995.

Godfrey, N. J., B. C. Beaudoin, S. L. Klemperer, and The 1993 Mendocino Working Group, Ophiolitic basement of the Great Valley forearc basin, California, from seismic and gravity data: Implications for crustal growth at the North American continental margin, *Geol. Soc. Am. Bull*., *109*, 1536–1562, 1997.

Godfrey, N. J., A. S. Meltzer, S. L. Klemperer, A. M. Trehu, B. Leitner, S. H. Clarke, and A. Ondrus, Evolution of the Gorda Escarpment, San Andreas fault and Mendocino triple junction from multichannel seismic data collected across the northern Vizcaino block, offshore northern California, *J. Geophys. Res*., *103*, 23,813–23,825, 1998.

Godson, R. H., Preparation of a digital grid of gravity anomaly values of the conterminous United States, in *The Utility of Regional Gravity and Magnetic Anomaly Maps*, edited by W. J. Hinze, pp. 38–45, Soc. of Explor. Geophys., Tulsa, Okla., 1985.

Griscom, A., and R. C. Jachens, Crustal and lithospheric structure from gravity and magnetic studies, in *The San Andreas Fault System, California*, edited by R. E. Wallace, *U.S. Geol. Surv. Prof. Pap*., *1515*, 239–260, 1990.

Griscom, A., R. C. Jachens, P. F. Halvorson, and R. J. Blakely, Regional geophysical setting of gold deposits in the Clear Lake region, California, in *Active Geothermal Systems and Gold-Mercury Deposits in the Sonoma-Clear Lake Volcanic Fields, California*, edited by J. J. Rytuba, pp. 289–311, Soc. of Econ. Geol., Littleton, Colo., 1993.

Hamilton, W., Mesozoic California and the underflow of Pacific mantle, *Geol. Soc. Am. Bull*., *80*, 2409–2430, 1969.

Holbrook, W. S., and W. D. Mooney, The crustal structure of the axis of the Great Valley, California, from seismic refraction measurements, *Tectonophysics*, *140*, 49–63, 1987.

Humphreys, E. D., and R. W. Clayton, Tomographic image of the southern California mantle, *J. Geophys. Res*., *95*, 19,725–19,746, 1990.

Humphreys, E. D., and K. G. Dueker, Western U.S. upper mantle structure, *J. Geophys. Res*., *99*, 9615–9634, 1994a.

Humphreys, E. D., and K. G. Dueker, Physical state of the western U.S. upper mantle, *J. Geophys. Res*., *99*, 9635–9650, 1994b.

Humphreys, E. D., and B. H. Hager, A kinematic model for the late Cenozoic development of southern California crust and upper mantle, *J. Geophys. Res*., *95*, 19,747–19,762, 1990.

Irwin, W. P., Specific gravity of sandstones in the Franciscan and related upper Mesozoic formations of California, *U.S. Geol. Surv., Prof. Pap*., *424-B*, B189–B191, 1961.

Jachens, R. C., and A. Griscom, Three-dimensional geometry of the Gorda plate beneath northern California, *J. Geophys. Res*., *88*, 9375–9392, 1983.

Jachens, R. C., and C. Moring, Maps of the thickness of Cenozoic deposits and the isostatic residual gravity over basement for Nevada, *U.S. Geol. Surv. Open File Rep*., *90-404*, 15 pp., 1990.

Jachens, R. C., A. Griscom, and C. W. Roberts, Regional extent of Great Valley basement west of the Great Valley, California: Implications for extensive tectonic wedging in the California Coast Ranges, *J. Geophys. Res*., *100*, 12,769–12,790, 1995.

Kaban, M. K., P. Schwintzer, and S. A. Tikhotsky, A global isostatic gravity model of the Earth, *Geophys. J. Int*., *136*, 519–536, 1999.

Kennet, J. P., et al., Santa Barbara Basin, Site 893, *Proc. Oceanic Drill. Program*, *Initial Rep*., *146*, part 2, 45, 1994.

Lamanuzzi, V. D., Relative *Pn* travel-time residuals for stations in southern California, M. S. thesis, 117 pp., Univ. of South. Calif., Los Angeles, 1981.

Langenheim, V. E., and R. C. Jachens, Gravity data collected along the Los Angeles regional seismic experiment (LARSE) and preliminary model of regional density variations in basement rocks, southern California, *U.S. Geol. Surv. Open File Rep*., *96-682*, 25 pp., 1996.

McCulloh, T. H., Mass properties of sedimentary rocks and gravimetric effects of petroleum and natural-gas reservoirs, *U.S. Geol. Surv. Prof. Pap*., *528-A*, 50 pp., 1967.

McNutt, M., Compensation of oceanic topography: An application of the response function technique to the *Surveyor* area, *J. Geophys. Res*., *84*, 7589–7598, 1979.

Mooney, W. D., Seismic methods for determining earthquake source parameters and lithospheric structure, in *Geophysical Framework of the Continental United States*, edited by L. C. Pakiser and W. D. Mooney, *Mem. Geol. Soc. Am*., *172*, 11–34, 1989.

Mooney, W. D., and L. W. Braile, The seismic structure of the continental crust and upper mantle of North America, in *The Geology of North America*, vol. A, *The Geology of North America: An Overview*, edited by A. W. Bally and A. R. Palmer, pp. 39–52, Geol. Soc. of Am., Boulder, Colo., 1989.

Mooney, W. D., and C. S. Weaver, Regional crustal structure and tectonics of the Pacific coastal states: California, Oregon and Washington, in Geophysical Framework of the Continental United States, edited by L. C. Pakiser and W. D. Mooney, *Mem. Geol. Soc. Am*., *172*, 129–161, 1989.

Mooney, W. D., G. Laske, and T. G. Masters, CRUST 5.1: A global crustal model at 5° × 5°, *J. Geophys. Res*., *103*, 727–747, 1998.

Oliver, H. W. (Ed.), Interpretation of the Gravity Map of California and its Continental Margin, 52 pp., *Bull. Calif. Div. Mines Geol*., *205*, 1980.

Oliver, H. W., J. G. Moore, and R. F. Sikora, Internal structure of the Sierra Nevada batholith based on specific gravity and gravity measurements, *Geophys. Res. Lett*., *20*, 2179–2182, 1993.

Raikes, S. A., Regional variations in upper mantle structure beneath southern California, *Geophys. J. R. Astron. Soc*., *63*, 187–216, 1980.

Ramirez, V. R., Evolution of the Coast Range Thrust as interpreted from seismic reflection data (abstract), *Geol. Soc. Am*., *Abstr. Programs*, *25*, 136, 1993.

Richards-Dinger, K. B., and P. M. Shearer, Estimating crustal thickness in southern California by stacking *PmP* arrivals, *J. Geophys. Res*., *102*, 15,211–15,224, 1997.

Ruppert, S., M. M. Fliedner, and G. Zandt, Thin crust and active upper mantle beneath the southern Sierra Nevada in the western United States, *Tectonophysics*, *286*, 237–252, 1998.

Sheffels, B., and M. McNutt, Role of subsurface loads and regional compensation in the isostatic balance of the Transverse Ranges, California: Evidence for intracontinental subduction, *J. Geophys. Res*., *91*, 6419–6431, 1986.

Simpson, R. W., R. C. Jachens, R. J. Blakely, and R. W. Saltus, A new isostatic residual gravity map of the conterminous United States with a discussion on the significance of isostatic residual anomalies, *J. Geophys. Res*., *91*, 8348–8372, 1986.

Strakhov, V. N., T. V. Romaniuk, and N. K. Frolova, Method of direct gravity problem solution for modeling of global and regional gravity anomalies, (in Russian), in *New Methods of the Gravity and Magnetic Anomaly Interpretation*, pp. 118–235, Inst. of the Phys. of the Earth, Moscow, 1989.

Thompson, G. A., R. Catchings, E. Goodwin, S. Holbrook, C. Jarchow, C. Mann, J. McCarthy, and D. Okaya, Geophysics of the western Basin and Range Province, in *Geophysical Framework of the Continental United States*, edited by L. C. Pakiser and W. D. Mooney, *Mem. Geol. Soc. Am*., *172*, 177–204, 1989.

M. K. Kaban and W. D. Mooney, U.S. Geological Survey, MS 977, 345 Middlefield Road, Menlo Park, CA 94025. (misha@kaban.msk.ru or mkaban@swave.wr.usgs.gov; mooney@usgs.gov)

(Received February 23, 1999; revised February 16, 2000; accepted June 23, 2000.)